PHYSICAL REVIEW D **94,** 055031 (2016)

Searching for singlino-Higgsino dark matter in the NMSSM

Qian-Fei Xiang,[1] Xiao-Jun Bi,[1] Peng-Fei Yin,[1] and Zhao-Huan Yu[2]

[1]*Key Laboratory of Particle Astrophysics, Institute of High Energy Physics, Chinese Academy of Sciences, Beijing 100049, China*

[2]*ARC Centre of Excellence for Particle Physics at the Terascale, School of Physics, The University of Melbourne, Victoria 3010, Australia*

(Received 14 June 2016; published 26 September 2016)

We study a simplified scenario in the next-to-minimal supersymmetric standard model with a split electroweak spectrum, in which only the singlino and Higgsinos are light and other superpartners are decoupled. Serving as a dark matter candidate, a singlino-dominated neutralino $\tilde{\chi}_1^0$ should have either resonant annihilation effects or sizable Higgsino components to satisfy the observed relic abundance. The sensitivities of LHC searches and dark matter detection experiments are investigated. With an integrated luminosity of $30(300)$ fb^{-1}, $3l + \not{E}_{\mathrm{T}}$ and $2l + \not{E}_{\mathrm{T}}$ searches at the 13 (14) TeV LHC are expected to reach up to $m_{\tilde{\chi}_1^0} \sim 150(230)$ GeV and $m_{\tilde{\chi}_2^0 \tilde{\chi}_1^\pm} \sim 320(480)$ GeV. Near future dark matter direct and indirect detection experiments are promising to cover the parameter regions where collider searches lose their sensitivities.

DOI: 10.1103/PhysRevD.94.055031

I. INTRODUCTION

With the discovery of the Higgs boson at the Large Hadron Collider (LHC) [1,2], the complete particle content of the standard model (SM) has been experimentally confirmed. However, the large radiative correction to the Higgs mass term leads to the hierarchy problem, which implies that there should be new physics between the electroweak scale and the Planck scale. In addition, the SM cannot explain the existence of dark matter (DM) in the Universe. Therefore, new particles like the DM candidate are required in new physics beyond the SM. Among numerous new physics scenarios, supersymmetry (SUSY) provides an elegant solution to the hierarchy problem by introducing the contributions to the Higgs mass term from superpartners. Moreover, the lightest supersymmetric particle (LSP) in the R-parity conserved SUSY models is absolutely stable and could be an excellent DM candidate.

The SUSY extension with the minimal field content is known as the minimal supersymmetric standard model (MSSM), which has many attractive features but also faces some challenges. For instance, the reason why the dimensional parameter μ in the supersymmetric mass term $\mu \hat{H}_u \hat{H}_d$ is far below the Planck scale is not explained in the MSSM. This is the well-known "μ-problem" [3]. Moreover, the mass of the lighter CP-even neutral Higgs boson is subject to a constraint, $m_h^2 \leq m_Z^2 \cos^2 2\beta$, at the tree level. Although loop effects can lift the mass up to $\sim$125 GeV to meet with the observed value, it is somewhat fine-tuned [4] and puts some constraints on the particle spectrum. For instance, the third generation squarks are required to be light in the SUSY (see, e.g., [5–8]).

The next-to-minimal supersymmetric standard model (NMSSM) solves the μ-problem by adding a singlet chiral superfield $\hat{S}$ to the MSSM (see Refs. [9,10] for recent reviews). As a result, μ is replaced by a dynamical quantity $\mu_{\mathrm{eff}} = \lambda v_s$ when S develops a vacuum expectation value (VEV) v_s, which is naturally at the electroweak scale. Furthermore, the mass of the SM-like Higgs boson can be easily interpreted due to the enlarged Higgs sector, which contains three CP-even neutral Higgs bosons, two CP-odd neutral Higgs bosons, and two charged Higgs bosons.

Since no superpartner has been found, SUSY searches at the LHC have set stringent constraints on the masses of superpartners. In particular, the masses of gluinos and the first two generations of squarks are required to be much higher than 1 TeV [11–13]. The constraints on the masses of neutralinos and charginos are much weaker due to the small electroweak production cross sections. For instance, in the case of pure wino $\tilde{\chi}_2^0$ and $\tilde{\chi}_1^\pm$ with pure bino $\tilde{\chi}_1^0$, the ATLAS limit $m_{\tilde{\chi}_2^0} \gtrsim 350$ GeV is obtained for $m_{\tilde{\chi}_1^0} \lesssim 100$ GeV, assuming $\mathrm{BR}(\tilde{\chi}_2^0 \to Z\tilde{\chi}_1^0) = 100\%$ [14]. Exclusion limits from other LHC searches for the electroweak superpartners can be found in Refs. [15–19]. These limits are derived in some simplified scenarios assumed. Thus, in a realistic MSSM they would be changed due to reduced branching ratios and modified kinematics [20–30,30–37]. In the NMSSM, neutralinos have additional singlino components $\tilde{S}$ from the fermionic part of $\hat{S}$. As a result, the interpretation of the LHC SUSY searches, as well as the DM phenomenology, would be affected (see, e.g., [38–45]).

In this work, we focus on the case where the LSP is a singlino-dominated neutralino (see, e.g., [46–51]). The mass hierarchy among the bino, winos, Higgsinos, and singlino is controlled by the diagonal elements of the neutralino mass matrix: M_1, M_2, μ_{eff}, and $2\kappa v_s$, where κ comes from the singlet self-interaction term $\frac{1}{3}\kappa \hat{S}^3$. Since the

 © 2016 American Physical Society

pure singlino DM would be overproduced in the early Universe due to the limited singlino interactions, the LSP $\tilde{\chi}_1^0$ should have some other components to provide an acceptable relic abundance for a standard cosmology. We can define three simplified scenarios for the singlino-dominated LSP: the singlino-bino scenario ($2\kappa v_s < M_1 \ll M_2,\ \mu_{\rm eff}$), the singlino-wino scenario ($2\kappa v_s < M_2 \ll M_1,\ \mu_{\rm eff}$), and the singlino-Higgsino scenario ($2\kappa v_s < \mu_{\rm eff} \ll M_1,\ M_2$). In these scenarios, some particular gauginos or Higgsinos with much higher masses decouple from the rest of the superpartners, leading to specific phenomenological consequences. Because there is no mixed mass term between the singlino and the bino/wino, the singlino can only mix with the bino/wino via Higgsino states. Therefore, $\tilde{\chi}_1^0$ has a very large singlino component in the singlino-bino and singlino-wino scenarios, and cannot easily explain the observed DM relic density.

In order to satisfy the observed relic density, the binolike LSP is usually required to be lighter than 100 GeV [52]. In the singlino-bino scenario, $\tilde{\chi}_1^0$ could be even lighter, e.g., $m_{\tilde{\chi}_1^0} \sim \mathcal{O}(10)$ GeV [38,41,53]. Although $\tilde{\chi}_1^0$ and $\tilde{\chi}_2^0$ can be quite light, the production rates of $\tilde{\chi}_1^0\tilde{\chi}_2^0$ and $\tilde{\chi}_2^0\tilde{\chi}_2^0$ at the LHC would still be very low compared with SM backgrounds. If other electroweak superpartners are too heavy, it is difficult to explore this scenario through electroweak production at the LHC. The singlino-wino scenario is analogous to the bino-wino scenario with a similar definition in the MSSM. In this scenario, the correct relic abundance could be achieved when coannihilation occurs between $\tilde{\chi}_1^0$ and $\tilde{\chi}_1^\pm/\tilde{\chi}_2^0$ in the early Universe, which requires a strong mass degeneracy. For such a squeezed spectrum, final state leptons from $\tilde{\chi}_1^\pm\tilde{\chi}_2^0$ production would be soft, and hence a hard initial state radiation jet could be helpful. For the bino-wino scenario, LHC $3l$ searches are expected to reach $m_{\tilde{\chi}_1^0} \sim 220(320)$ GeV for $m_{\tilde{\chi}_2^0} - m_{\tilde{\chi}_1^0} = 20(30)$ GeV at $\sqrt{s} = 14$ TeV with an integrated luminosity of 300 fb^{-1} [21]. These limits could be approximately applied to the singlino-wino scenario.

Below we only focus on the singlino-Higgsino scenario, where the LSP $\tilde{\chi}_1^0$ is mainly singlino, while $\tilde{\chi}_{2,3}^0$ and $\tilde{\chi}_1^\pm$ are mainly Higgsinos. Some recent works on this scenario include studies on LHC searches [46,47] and IceCube indirect searches [50]. In this work, first we investigate the viable parameter regions and decay patterns of neutralinos and charginos. Then we derive current bounds and future prospects of LHC searches, DM direct detection, and DM indirect detection. In order to have effective $\tilde{\chi}_1^0\tilde{\chi}_1^0$ annihilation in the early Universe, the mixture with Higgsinos and annihilation through a Higgs/Z boson resonance would be helpful [39,54]. Near the resonance regions, it is difficult to probe $\tilde{\chi}_1^0$ in direct detection experiments because the effective DM couplings to quarks might drop dramatically. As Higgsino-dominated $\tilde{\chi}_{2,3}^0$ and $\tilde{\chi}_1^\pm$ are light, LHC searches in the $3l + \not{E}_{\rm T}$ and $2l + \not{E}_{\rm T}$ final states are sensitive to DM signatures through $\tilde{\chi}_{2,3}^0\tilde{\chi}_1^\pm$ and $\tilde{\chi}_1^+\tilde{\chi}_1^-$ pair production processes, respectively. However, if the mass splitting between $\tilde{\chi}_{2,3}^0/\tilde{\chi}_1^\pm$ and $\tilde{\chi}_1^0$ is small, the LHC sensitivity would decrease due to the low reconstruction efficiency of soft leptons. In this case, because $\tilde{\chi}_1^0$ has moderate Higgsino components, it remains possible to probe DM in direct and indirect detection experiments.

This paper is organized as follows. In Sec. II we provide details and results of a parameter scan in the singlino-Higgsino scenario and present three typical benchmark points. Section III focuses on LHC searches in the $3l + \not{E}_{\rm T}$ and $2l + \not{E}_{\rm T}$ channels. In Sec. IV we investigate the sensitivity of DM detection experiments. Section V gives our conclusions and discussions.

II. PARAMETER SPACE SCAN

The Z_3-invariant NMSSM superpotential is [9,10]

$$W = W_{\rm MSSM} + \lambda \hat{S}\,\hat{H}_u\,\hat{H}_d + \frac{1}{3}\kappa\hat{S}^3, \tag{1}$$

where $W_{\rm MSSM}$ is the MSSM superpotential, and λ and κ are dimensionless couplings. Once S develops a VEV v_s, an effective μ-term, $\mu_{\rm eff}\hat{H}_u\,\hat{H}_d$, is generated with $\mu_{\rm eff} = \lambda v_s$. The soft breaking terms in the Higgs sector are given by

$$\begin{aligned} V_{\rm soft} &= m_{H_u}^2|H_u|^2 + m_{H_d}^2|H_d|^2 + m_S^2|S|^2 \\ &\quad + \left(\lambda A_\lambda S H_u H_d + \frac{1}{3}\kappa A_\kappa S^3 + \text{H.c.}\right). \end{aligned} \tag{2}$$

The minimization of the scalar potential relates the soft parameters $m_{H_u}^2$, $m_{H_d}^2$, and m_S^2 to m_Z, v_s, and $\tan\beta \equiv v_u/v_d$, where v_u and v_d are the VEVs of H_u and H_d. Therefore, the Higgs and Higgsino sectors in the NMSSM are determined by six parameters,

$$\lambda, \quad \kappa, \quad A_\lambda, \quad A_\kappa, \quad \mu_{\rm eff}, \quad \tan\beta. \tag{3}$$

In the gauge basis $\psi_\alpha = (\tilde{B}, \tilde{W}^0, \tilde{H}_d^0, \tilde{H}_u^0, \tilde{S})$, the neutralino mass term can be expressed as $-\frac{1}{2}[\psi_\alpha(M_{\tilde{\chi}^0})_{\alpha\beta}\psi_\beta + \text{H.c.}]$, where the symmetric mass matrix is

$$M_{\tilde{\chi}^0} = \begin{pmatrix} M_1 & 0 & -g_1 v_d/\sqrt{2} & g_1 v_u/\sqrt{2} & 0 \\ & M_2 & g_2 v_d/\sqrt{2} & -g_2 v_u/\sqrt{2} & 0 \\ & & 0 & -\mu_{\rm eff} & -\lambda v_u \\ & & & 0 & -\lambda v_d \\ & & & & 2\kappa v_s \end{pmatrix}. \tag{4}$$

It can be diagonalized by a mixing matrix N, and hence the mass eigenstates are related to the gauge eigenstates through

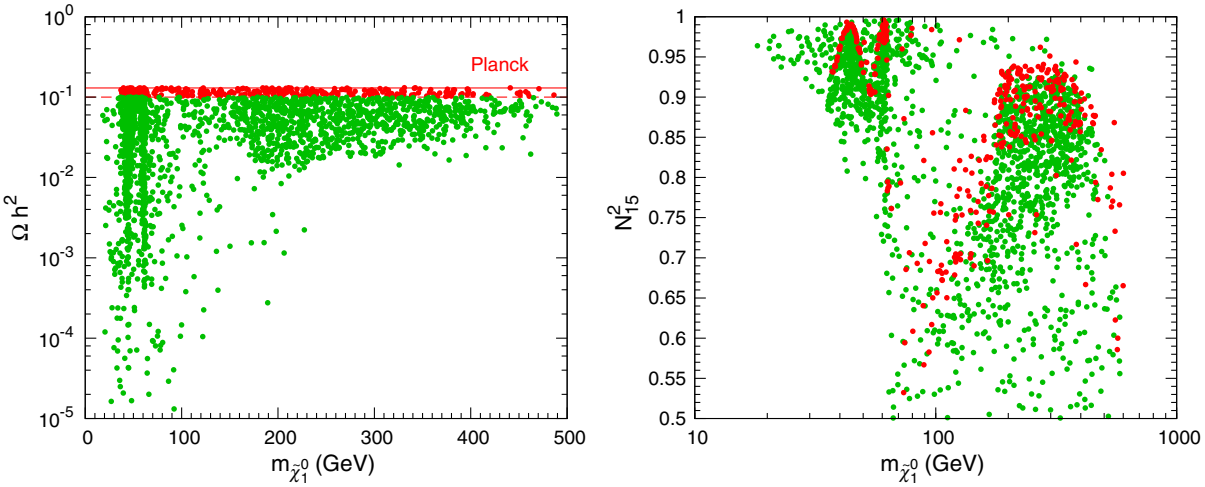

(a) $\Omega_{\tilde{\chi}_1^0}h^2$ vs. $m_{\tilde{\chi}_1^0}$ (b) $|N_{15}|^2$ vs. $m_{\tilde{\chi}_1^0}$

FIG. 1. DM relic density $\Omega_{\tilde{\chi}_1^0}h^2$ (a) and singlino component $|N_{15}|^2$ (b) versus the LSP mass $m_{\tilde{\chi}_1^0}$. All points satisfy $\Omega_{\tilde{\chi}_1^0}h^2 < 0.131$, while the red points also satisfy $\Omega_{\tilde{\chi}_1^0}h^2 > 0.107$.

$$\tilde{\chi}_i^0 = N_{i1}\tilde{B} + N_{i2}\tilde{W}^0 + N_{i3}\tilde{H}_d^0 + N_{i4}\tilde{H}_u^0 + N_{i5}\tilde{S}. \quad (5)$$

For the singlino-Higgsino scenario, we perform a random scan to identify the NMSSM parameter points that satisfy the observed DM relic density. In order to reduce the number of free parameters, we fix M_1, M_2, and M_3 to be 2, 2, and 5 TeV, respectively. Moreover, all trilinear couplings and soft mass terms for squarks and sleptons are set to be 5 TeV. Thus, the bino, winos, gluinos, squarks, and sleptons are heavy and decouple from the physics we concern. The remaining free parameters are related to the Higgs and Higgsino sectors. We carry out a random scan within the following ranges:

$$100\ \text{GeV} \le \mu_{\text{eff}} \le 600\ \text{GeV}, \qquad -1\ \text{TeV} \le A_\kappa \le 0,$$
$$100\ \text{GeV} \le A_\lambda \le 10\ \text{TeV}, \quad (6)$$

$$1 \le \tan\beta \le 50, \quad 0.05 \le \lambda \le 0.7, \quad 0.05 \le \kappa \le 0.7. \quad (7)$$

Here we require that the singlino-dominated $\tilde{\chi}_1^0$ should satisfy $|N_{15}|^2 > 0.5$. A recent comprehensive study on the allowed NMSSM parameter space can be found in Ref. [55].

We employ the package `NMSSMTools 4.6.0` [56–58] for calculating particle spectra, decay branching ratios, and many other observables. DM relic density, direct detection, and indirect detection results are computed through the embedded `micrOMEGAs 3` code [59]. During the scan, several constraints are imposed as follows.

DM relic density The $\tilde{\chi}_1^0$ relic density $\Omega_{\tilde{\chi}_1^0}h^2$ is required to be below 0.131, consistent with the latest Planck measurement [60].

Higgs bounds One of the Higgs scalars should be SM-like and its mass should be within the range of 122–128 GeV.[1] Its couplings to other SM particles should be consistent with the results derived from a global fit to the measurements of the Higgs partial decay widths within 3σ derivations (see, e.g., [61]).

LEP bounds Direct SUSY searches at the Large Electron-Positron Collider (LEP) have set bounds on superpartners. Here we impose two relevant bounds. One is that the lighter chargino should satisfy $m_{\tilde{\chi}_1^\pm} > 103.5$ GeV, which is determined by the LEP collision energy. The other one is that the Z invisible width should satisfy $\Gamma_Z^{\text{inv}} < 2$ MeV at 95% C.L. [62]. When the decay channel into $\tilde{\chi}_1^0\tilde{\chi}_1^0$ opens, this width may exceed the experimental value.

Muon a light Higgs boson would significantly affect the muon anomalous magnetic moment $a_\mu = (g_\mu - 2)/2$, whose most accurate measurement comes from the E821 experiment [63]. Here we require the NMSSM contribution within the 3σ derivation, i.e., $-5.62 \times 10^{-11} < a_\mu^{\text{NMSSM}} < 5.54 \times 10^{-9}$.

B physics bounds There are flavor constraints from B meson rare decays, such as $B_s \to \mu^+\mu^-$, $B^+ \to \tau^+\nu$, and $B_s \to X_s\gamma$. We use the recent experimental results at 95% C.L.: $1.7 \times 10^{-9} < \text{BR}(B_s \to \mu^+\mu^-) < 4.5 \times 10^{-9}$ [64], $0.85 \times 10^{-4} < \text{BR}(B^+ \to \tau^+\nu) < 2.89 \times 10^{-4}$ [65], and $2.99 \times 10^{-4} < \text{BR}(B_s \to X_s\gamma) < 3.87 \times 10^{-4}$ [64].

[1]Here we adopt a default setting of NMSSMTools (*Option 8 0*) to calculate the Higgs masses without including the full loop corrections. Once these corrections to Higgs masses are considered [*Option 8 2* for the full one-loop corrections and the two-loop $\mathcal{O}(\alpha_t\alpha_s + \alpha_b\alpha_s)$ corrections], some benchmark points we selected might not satisfy all the Higgs bounds.

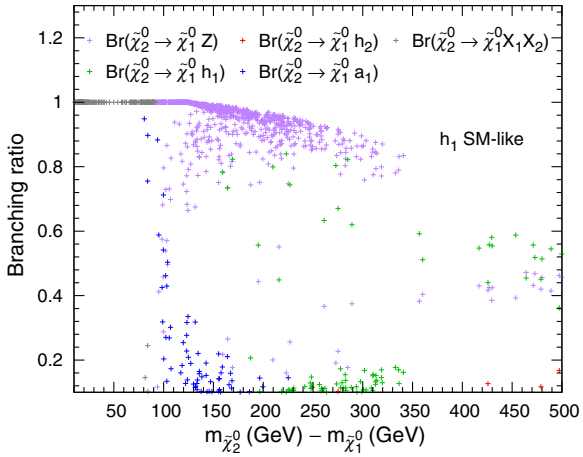

(a) $\tilde{\chi}_2^0$ decay branching ratios , h_1 is SM-like Higgs boson

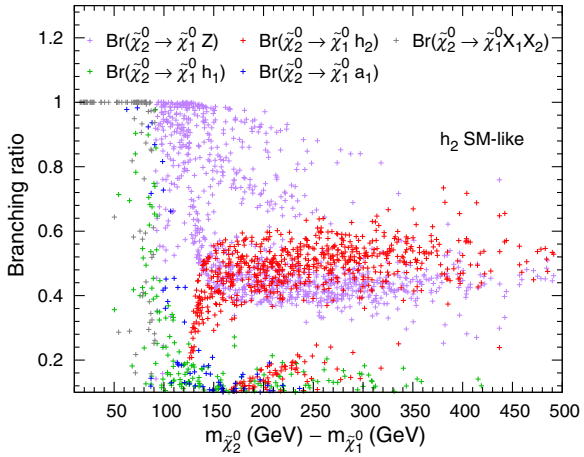

(b) $\tilde{\chi}_2^0$ decay branching ratios , h_2 is SM-like Higgs boson

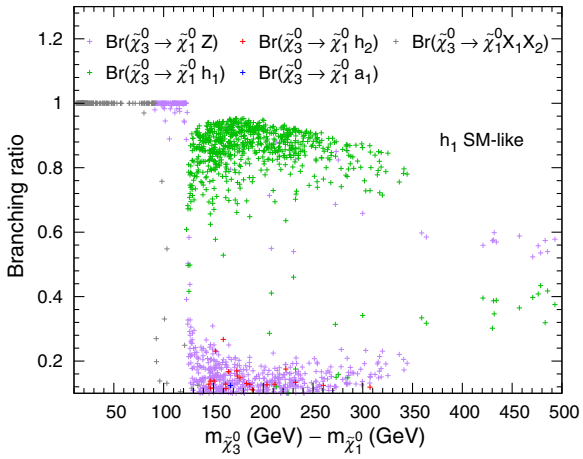

(c) $\tilde{\chi}_3^0$ decay branching ratios , h_1 is SM-like Higgs boson

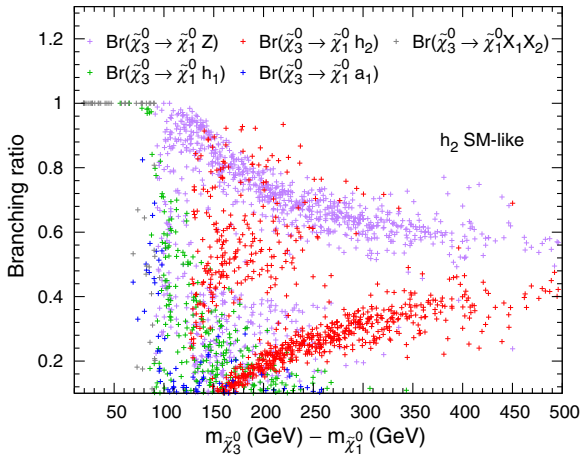

(d) $\tilde{\chi}_3^0$ decay branching ratios , h_2 is SM-like Higgs boson

FIG. 2. Decay branching ratios of $\tilde{\chi}_2^0$ and $\tilde{\chi}_3^0$ for h_1 or h_2 are the SM-like Higgs boson. Purple, green, red, and blue points correspond to decays into $\tilde{\chi}_1^0 Z$, $\tilde{\chi}_1^0 h_1$, $\tilde{\chi}_1^0 h_2$, and $\tilde{\chi}_1^0 a_1$, respectively. Gray points represent three-body decay branching ratios.

Now we analyze the properties of the parameter points survived from the above constraints. Figure 1 shows the calculated $\tilde{\chi}_1^0$ relic density for a standard cosmology. The red points can saturate the observed relic abundance ($0.107 < \Omega_{\tilde{\chi}_1^0} h^2 < 1.131$), while the green points predict a lower abundance ($\Omega_{\tilde{\chi}_1^0} h^2 < 0.107$), which may be compensated by other production mechanisms, e.g., nonthermal production [66–68] and cosmological enhancement due to the quintessential effect [69–71]. Another possibility is that $\tilde{\chi}_1^0$ may just constitute a fraction of the whole DM [72]. Figure 1(b) shows $|N_{15}|^2$, the squared singlino component of $\tilde{\chi}_1^0$. This confirms that the survived points truly correspond to singlino-dominated $\tilde{\chi}_1^0$.

Two bunches of points gather around $m_{\tilde{\chi}_1^0} \sim 45$ and $\sim$60 GeV, corresponding to resonance enhancements of the Z boson and the SM-like Higgs boson for $\tilde{\chi}_1^0 \tilde{\chi}_1^0$ annihilation, respectively. There are also some scattered points yielding a very low relic density, due to resonance enhancements of other Higgs scalars, whose masses are undetermined. In addition, most of the points with $m_{\tilde{\chi}_1^0} \gtrsim 70$ GeV do not have resonance effects. In this case, $\tilde{\chi}_1^0$ has larger Higgsino components and a smaller singlino component.

In Fig. 2 we present branching ratios of $\tilde{\chi}_2^0$ [Figs. 2(a) and 2(b)] and $\tilde{\chi}_3^0$ [Figs. 2(c) and 2(d)] decaying into $\tilde{\chi}_1^0$ versus mass differences $m_{\tilde{\chi}_2^0} - m_{\tilde{\chi}_1^0}$ and $m_{\tilde{\chi}_3^0} - m_{\tilde{\chi}_1^0}$, respectively. These ratios affect the LHC discovery possibility of the parent particles. Here we illustrate four typical decay channels, $\tilde{\chi}_1^0 Z$, $\tilde{\chi}_1^0 h_1$, $\tilde{\chi}_1^0 h_2$, and $\tilde{\chi}_1^0 a_1$. We also show three-body decay branching ratios of $\tilde{\chi}_2^0$ and $\tilde{\chi}_3^0$ in Fig. 2. These decay modes are typically dominant when $m_{\tilde{\chi}_{2,3}^0} - m_{\tilde{\chi}_1^0} < m_Z$ for $\kappa/\lambda \gtrsim 0.4$. If the decay channels into

TABLE I. Information of benchmark points. $\tilde{\chi}_1^0 X$ means $\tilde{\chi}_1^0$ associated with the particle(s) indicated in the entries. $q\bar{q}$, $l\bar{l}$, and $v_l\bar{v}_l$ represent the sums over quarks, charged leptons, and neutrinos, respectively.

	BP1	BP2	BP3
λ, κ	0.091, 0.016	0.270, 0.100	0.368, 0.144
$\tan\beta$, $\mu_{\rm eff}$ (GeV)	39.6, 163.3	35.1, 121.3	35.6, 121.0
A_κ (GeV), A_λ (TeV)	−35.9, 8.94	−173.4, 3.79	−8.77, 4.43
$m_{\tilde{\chi}_1^0}$ (GeV)	59.6	77.0	71.7
$m_{\tilde{\chi}_2^0}, m_{\tilde{\chi}_3^0}, m_{\tilde{\chi}_1^\pm}$ (GeV)	169, 173, 170	134, 146, 126	137, 160, 126
$m_{h_1}, m_{h_2}, m_{a_1}$ (GeV)	46.0, 126, 55.8	23.0, 125, 153	95.3, 125, 38.7
$\lvert N_{13}\rvert^2 + \lvert N_{14}\rvert^2$, $\lvert N_{15}\rvert^2$	1.3%, 98.7%	33.2%, 66.8%	43.5%, 56.4%
$\Omega_{\tilde{\chi}_1^0}h^2$	0.120	0.059	0.067
BR($\tilde{\chi}_2^0 \to \tilde{\chi}_1^0 X$)	Z 98.7%	h_1 84.4%, $q\bar{q}$ 10.6% $l\bar{l}$ 3%, $v_l\bar{v}_l$ 3%	a_1 98.6%
BR($\tilde{\chi}_3^0 \to \tilde{\chi}_1^0 X$)	Z 97.1% a_1 2.7%	h_1 100%	a_1 73.2%, $q\bar{q}$ 14% $l\bar{l}$ 2%, $v_l\bar{v}_l$ 4%
BR($h_1/a_1 \to b\bar{b}/\tau^+\tau^-$)	/	$h_1 \to b\bar{b}$ 91.8% $h_1 \to \tau^+\tau^-$ 7.3%	$a_1 \to b\bar{b}$ 91.8% $a_1 \to \tau^+\tau^-$ 7.7%

$\tilde{\chi}_1^0$ and the SM-like Higgs boson are kinematically allowed, they would be sizable, and even dominant for $\tilde{\chi}_3^0$ decays. BR($\tilde{\chi}_{2,3}^0 \to \tilde{\chi}_1^0 a_1$) deceases as the mass differences increase, becoming negligible when $m_{\tilde{\chi}_{2,3}^0} - m_{\tilde{\chi}_1^0} \gtrsim 150$ GeV.

We pick up three benchmark points to represent typical cases, as listed in Table I. The dominant $\tilde{\chi}_2^0$ decay channel in BP1 is $\tilde{\chi}_2^0 \to \tilde{\chi}_1^0 Z$. This is the most probable case, as we can see from Figs. 2(a) and 2(b). On the other hand, $\tilde{\chi}_2^0$ in BP2 and BP3 mainly decays into $\tilde{\chi}_1^0 h_1$ and $\tilde{\chi}_1^0 a_1$, respectively, because the $\tilde{\chi}_1^0 Z$ channel is kinematically forbidden. In these benchmark points, h_1 and a_1 are almost pure singlet scalars. $\tilde{\chi}_1^0$ in BP1 is almost pure singlino, but it could still effectively annihilate to give a correct relic abundance with its tiny Higgsino components, due to the Higgs resonance enhancement. Although the dominant decay channels of $\tilde{\chi}_2^0$ and $\tilde{\chi}_3^0$ in BP2 and BP3 are different ($\tilde{\chi}_1^0 h_1$ and $\tilde{\chi}_1^0 a_1$), their production signatures may be similar, as h_1 and a_1 have analogous decays (∼92% into $b\bar{b}$ and ∼7% into $\tau^+\tau^-$). In addition, $\tilde{\chi}_1^\pm$ in BP2 and BP3 can only decay into off-shell W bosons, leading to softer visible products compared with BP1.

III. LHC SEARCHES

Compared with colored superpartners, the production of electroweak superpartners at the LHC yields much lower rates. A helpful search strategy is to make use of ≥ 2 charged leptons produced in decays of neutralinos, charginos, and sleptons. SM backgrounds in these multilepton channels are quite clean.

With an integrated luminosity of ∼20 fb^{-1} at the 8 TeV LHC, both the ATLAS and CMS collaborations reported their search results for MSSM charginos and neutralinos in the $3l + \not{E}_{\rm T}$ [14,18] and $2l + \not{E}_{\rm T}$ [15] final states. The $3l + \not{E}_{\rm T}$ search is particularly sensitive to $\tilde{\chi}_1^\pm \tilde{\chi}_{2,3}^0$ production, which is a major process of electroweak SUSY production. Assuming $\tilde{\chi}_1^\pm$ and $\tilde{\chi}_2^0$ are both pure wino with BR($\tilde{\chi}_1^\pm \to \tilde{\chi}_1^0 W^{\pm(*)}$) = BR($\tilde{\chi}_2^0 \to \tilde{\chi}_1^0 Z^{(*)}$) = 100%, the ATLAS analysis has excluded $m_{\tilde{\chi}_1^\pm}$ and $m_{\tilde{\chi}_2^0}$ up to ∼350 GeV at 95% C.L. The $2l + \not{E}_{\rm T}$ channel can be used to search for the $\tilde{\chi}_1^+ \tilde{\chi}_1^-$ production, but it is less sensitive, just excluding $m_{\tilde{\chi}_1^\pm}$ up to ∼180 GeV at 95% C.L.

In the singlino-Higgsino scenario, $\tilde{\chi}_1^\pm$, $\tilde{\chi}_2^0$, and $\tilde{\chi}_3^0$ are Higgsino dominated. We consider the production processes $pp \to \tilde{\chi}_{2,3}^0 \tilde{\chi}_{2,3}^0$, $\tilde{\chi}_{2,3}^0 \tilde{\chi}_1^\pm$, and $\tilde{\chi}_1^+ \tilde{\chi}_1^-$ at the LHC. $\tilde{\chi}_2^0$ and $\tilde{\chi}_3^0$ can decay into $\tilde{\chi}_1^0 Z^{(*)}$, $\tilde{\chi}_1^0 h_{1,2}^{(*)}$, and $\tilde{\chi}_1^0 a_1^{(*)}$, while $\tilde{\chi}_1^\pm$ basically decays into $\tilde{\chi}_1^0 W^{\pm(*)}$. Because the doublet (Higgsino) coupling to W is weaker than the triplet (wino) coupling, the production rates of $\tilde{\chi}_1^\pm \tilde{\chi}_2^0$ and $\tilde{\chi}_1^\pm \tilde{\chi}_3^0$ here are much lower than the $\tilde{\chi}_1^\pm \tilde{\chi}_2^0$ production rate in the pure wino case. Moreover, decays into $\tilde{\chi}_1^0$ and a Higgs scalar cannot be neglected and they hardly contribute to the trilepton final state as the scalar mainly decays into $b\bar{b}$. Therefore, constraints from the $3l + \not{E}_{\rm T}$ searches are expected to be weaker than the pure wino case. This situation is similar to that in the bino-Higgsino scenario [26].

In order to evaluate the current constraints, we recast the ATLAS $3l + \not{E}_{\rm T}$ [14] and $2l + \not{E}_{\rm T}$ [15] analyses to the singlino-Higgsino scenario based on a Monte Carlo simulation. In the simulation, we use `MadGraph 5` [73] to generate background and signal samples, and use `PYTHIA 6` [74] to deal with the parton shower, particle decay, and hadronization processes. The MLM scheme [75] is employed to handle the matching between matrix element and parton shower calculations. `Delphes 3` [76] is utilized to carry out a fast detection simulation with the ATLAS setup. Jets are clustered using the anti-$k_{\rm T}$ algorithm [77] with a radius parameter of $R = 0.4$.

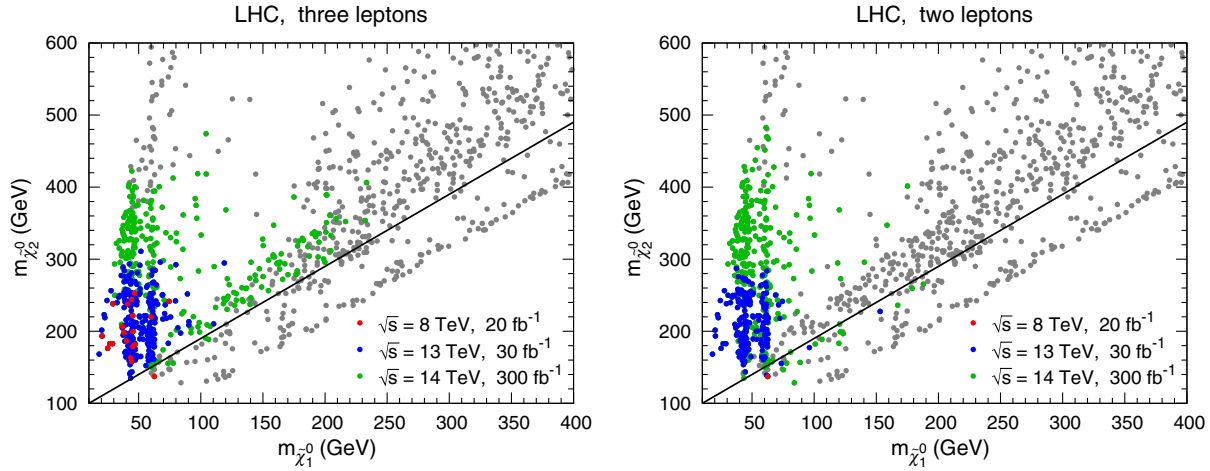

(a) $3l + \not{E}_{\mathrm{T}}$ channel (b) $2l + \not{E}_{\mathrm{T}}$ channel

FIG. 3. 95% C.L. exclusion results of the $3l + \not{E}_{\mathrm{T}}$ (a) and $2l + \not{E}_{\mathrm{T}}$ (b) searches in the $m_{\tilde{\chi}_1^0} - m_{\tilde{\chi}_2^0}$ plane. Red points are excluded by the 8 TeV ATLAS analyses with ~20 fb^{-1} data. Blue (green) points are expected to be excluded by the 13 TeV (14 TeV) LHC with an integrated luminosity of 30 fb^{-1} (300 fb^{-1}). Gray points survive from the above searches. The solid black lines denote the threshold $m_{\tilde{\chi}_2^0} = m_{\tilde{\chi}_1^0} + m_Z$.

We generate simulation samples for $\tilde{\chi}_{2,3}^0\tilde{\chi}_{2,3}^0$, $\tilde{\chi}_{2,3}^0\tilde{\chi}_1^\pm$, and $\tilde{\chi}_1^+\tilde{\chi}_1^-$ production and apply the same cuts in various signal regions of the ATLAS analyses. The exclusion limits projected in the $m_{\tilde{\chi}_1^0} - m_{\tilde{\chi}_2^0}$ plane are shown in Fig. 3, where the red points are excluded at 95% C.L. Since both $\tilde{\chi}_2^0$ and $\tilde{\chi}_1^\pm$ are almost pure Higgsinos, their masses are close, determined by μ_{eff}. We find that the ATLAS $3l + \not{E}_{\mathrm{T}}$ searches have excluded $m_{\tilde{\chi}_2^0,\tilde{\chi}_1^\pm}$ up to ~250 GeV, which is roughly 100 GeV lower than the pure wino case [14]. The $2l + \not{E}_{\mathrm{T}}$ constraints would be even weaker. Below we turn to evaluating the LHC sensitivities at $\sqrt{s} = 13$ and 14 TeV.

A. Prospect in the $3l + \not{E}_{\mathrm{T}}$ channel

In the $3l + \not{E}_{\mathrm{T}}$ search channel, dominant SM backgrounds are WZ and ZZ production. Minor backgrounds include $t\bar{t}$, $t\bar{t}V$ ($V = W$, Z), tZ, VVV, Higgs production, and so on. We omit these minor backgrounds for simplicity. In order to efficiently suppress backgrounds and increase the signal significance, we adopt the following selection cuts. Hereafter a charged lepton l denotes an electron or a muon.

Basic cuts Select the events with exactly three charged leptons that satisfy $p_{\mathrm{T}} > 20$ GeV and $|\eta| < 2.5$ and are separate from each other by $\Delta R > 0.3$; veto the events containing a b-jet with $p_{\mathrm{T}} > 30$ GeV and $|\eta| < 2.5$; select the events with $|m_{\mathrm{SFOS}} - m_Z| < 10$ GeV.

[$\not{E}_{\mathrm{T}}$ *cut*] Select the events with $\not{E}_{\mathrm{T}} > 50$ or 100 GeV.

[m_{T} *cut*] Select the events with $m_{\mathrm{T}} > 100$ GeV.

Here m_{SFOS} is the invariant mass of a same-flavor opposite-sign (SFOS) lepton pair. When there are two such pairs, we choose the one with an invariant mass closer to m_Z. Events without an SFOS pair are discarded. m_{T} is the transverse mass defined as $m_{\mathrm{T}} = \sqrt{2(p_{\mathrm{T}}^l \not{E}_{\mathrm{T}} - \mathbf{p}_{\mathrm{T}}^l \cdot \mathbf{p}_{\mathrm{T}}^{\mathrm{miss}})}$, where $\mathbf{p}_{\mathrm{T}}^{\mathrm{miss}}$ is the missing transverse momentum vector and the lepton l is the one not forming the SFOS lepton pair. For the $\not{E}_{\mathrm{T}}$ cut, we adopt two thresholds, 50 and 100 GeV, optimized for light and heavy $m_{\tilde{\chi}_2^0,\tilde{\chi}_1^\pm}$, respectively.

In Fig. 4, we demonstrate the m_{SFOS}, $\not{E}_{\mathrm{T}}$, and m_{T} distributions of backgrounds and signals after the basic cuts except $|m_{\mathrm{SFOS}} - m_Z| < 10$ GeV. The m_{SFOS} variable is chiefly used to reconstruct Z bosons from their l^+l^- products. Therefore, there is a clear peak near m_Z in the m_{SFOS} distributions for WZ and ZZ, as well as that for the signal BP1 where both $\tilde{\chi}_2^0$ and $\tilde{\chi}_3^0$ dominantly decay into $\tilde{\chi}_1^0 Z$. On the other hand, both $\tilde{\chi}_2^0$ and $\tilde{\chi}_3^0$ in BP2 and BP3 primarily decay into $\tilde{\chi}_1^0$ and a Higgs boson (h_1 or a_1), which subsequently decay into $\tau^+\tau^-$ with a branching ratio lower than 10%. Thus, the peaks in the m_{SFOS} distributions for BP2 and BP3 are not at m_Z. One reason for this is that the relevant decay products h_1 and a_1 are typically lighter than Z. Another one is that electrons and muons from tau leptonic decays have lower energies due to the associated neutrinos. Therefore, the cut condition $|m_{\mathrm{SFOS}} - m_Z| < 10$ GeV is only optimized for the case like BP1.

The $3l$ final state from the ZZ background mainly comes from the case that both Z bosons decay into l^+l^- pairs but one lepton cannot be successfully reconstructed. In this case there is no neutrino contributing $\not{E}_{\mathrm{T}}$. Thus its $\not{E}_{\mathrm{T}}$ distribution is softer than others, and so is its m_{T} distribution. For the WZ background, the m_{T} variable is bounded by the W boson mass; hence the distribution has an obvious endpoint near m_W.

Table II lists visible cross sections of backgrounds and signals as well as signal significances assuming

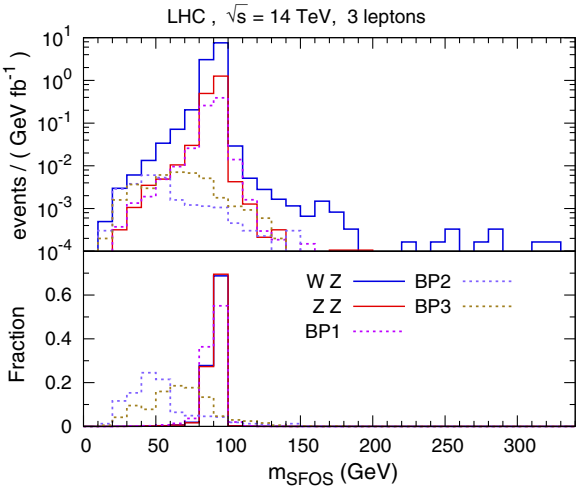

(a) m_{SFOS} distributions

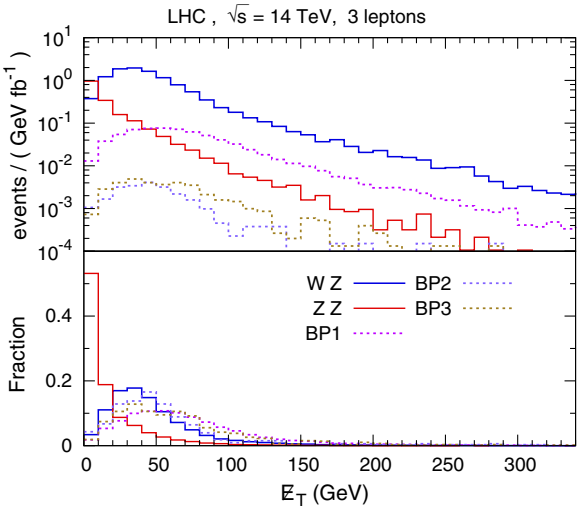

(b) $\not{E}_{\mathrm{T}}$ distributions

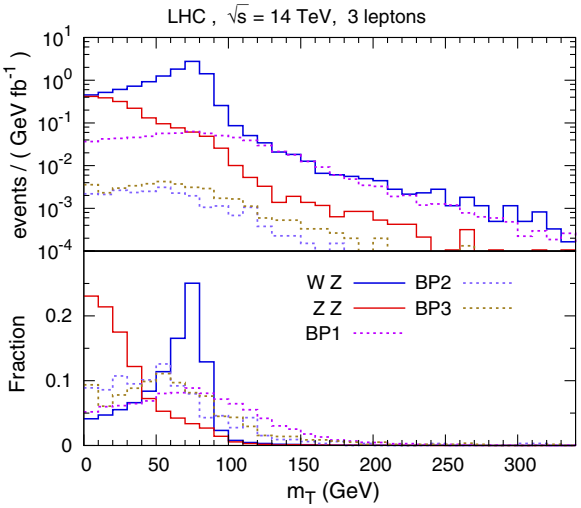

(c) m_{T} distributions

FIG. 4. m_{SFOS} (a), $\not{E}_{\mathrm{T}}$ (b), and m_{T} (c) distributions for backgrounds and signal benchmark points in the $3l + \not{E}_{\mathrm{T}}$ channel at the 14 TeV LHC.

$\sqrt{s} = 14$ TeV and an integrated luminosity of 300 fb^{-1} after each cut. Here the visible cross section is defined as the production cross section multiplied by the acceptance and efficiency. The signal significance $\mathcal{S}$ is defined as $S/\sqrt{S + B + (0.1B)^2}$, with S (B) denoting the event number of signals (backgrounds). A 10% systematic uncertainty on the backgrounds has been considered in our analysis. We find that the $\not{E}_{\mathrm{T}} > 50$ GeV and $m_{\mathrm{T}} > 100$ GeV cuts suppress the WZ (ZZ) background by 2 (3) orders of magnitude. Consequently, the signal significance for BP1 is efficiently increased. It is expected to reach the 9.9σ significance with a data set of 300 fb^{-1}.

TABLE II. Visible cross sections σ (in fb) for backgrounds and signal benchmark points after each cut in the $3l + \not{E}_{\mathrm{T}}$ channel at the 14 TeV LHC. The signal significances ($\mathcal{S}$) assuming an integrated luminosity of 300 fb^{-1} are also listed.

	WZ	ZZ	BP1		BP2		BP3	
	σ	σ	σ	$\mathcal{S}$	σ	$\mathcal{S}$	σ	$\mathcal{S}$
Basic cuts	105	17.3	6.39	0.52	0.021	0.0017	0.060	0.0049
$\not{E}_{\mathrm{T}} > 50$ GeV	37.2	1.51	4.11	1.06	0.008	0.0021	0.034	0.0087
$m_{\mathrm{T}} > 100$ GeV	1.22	0.06	1.60	9.93	0.004	0.0278	0.014	0.0973

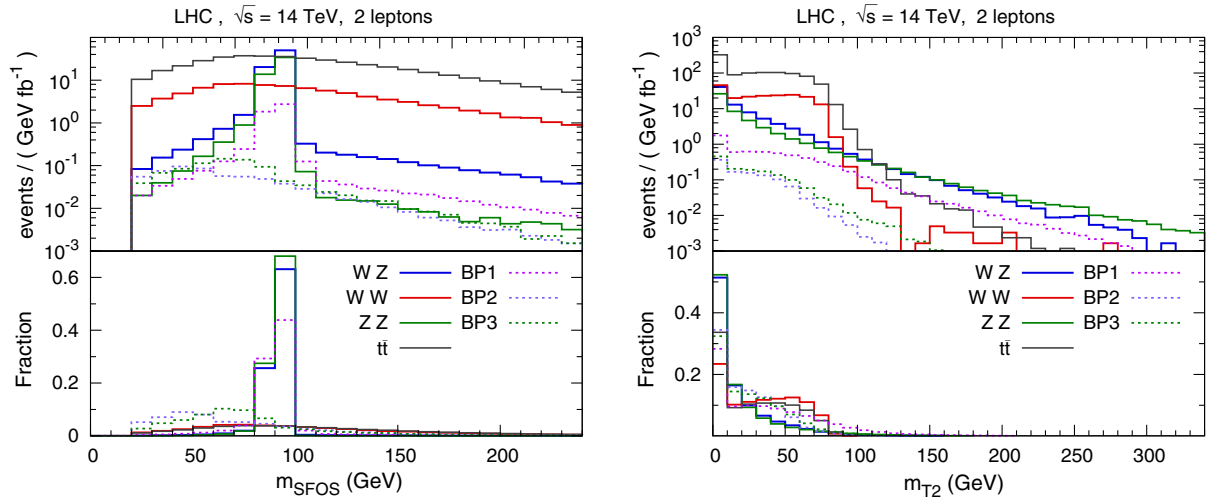

(a) m_{SFOS} distributions (b) m_{T2} distributions

FIG. 5. m_{SFOS} (a) and m_{T2} (b) distributions for backgrounds and signal benchmark points in the $2l + \not{E}_{\mathrm{T}}$ channel at the 14 TeV LHC.

The expected 95% C.L. exclusion results at the $\sqrt{s} = 13$ and 14 TeV have been presented in Fig. 3. With an integrated luminosity of 30(300) fb^{-1}, LHC searches are expected to reach up to $m_{\tilde{\chi}_2^0,\tilde{\chi}_1^\pm} \sim 320(420)$ GeV. There are many points with $m_{\tilde{\chi}_2^0} \lesssim m_{\tilde{\chi}_1^0} + m_Z$ that may not be explored even with a data set of 300 fb^{-1} at the 14 TeV LHC, because $\tilde{\chi}_2^0$ may have a small $\tilde{\chi}_1^0 Z$ branching ratio or decay into an off-shell Z boson.

B. Prospect in the $2l + \not{E}_{\mathrm{T}}$ channel

Major backgrounds in the $2l + \not{E}_{\mathrm{T}}$ channel are WW, WZ, ZZ, and $t\bar{t}$ production. The following selection cuts are used.

Basic cuts Select the events with exactly two opposite-sign charged leptons that satisfy $p_{\mathrm{T}} > 20$ GeV and $|\eta| < 2.5$; the harder lepton should have $p_{\mathrm{T}} > 30$ GeV; if the two leptons are the same flavor, their invariant mass should satisfy $m_{\mathrm{SFOS}} > 20$ GeV and $|m_{\mathrm{SFOS}} - m_Z| > 10$ GeV.

Jet veto Veto the events containing any jet with $p_{\mathrm{T}} > 30$ GeV and $|\eta| < 2.5$.

[m_{T2} *cut*] Select the events with $m_{\mathrm{T2}} > 90$, 120, or 150 GeV.

Note that the condition $m_{\mathrm{SFOS}} > 20$ GeV is used to avoid low mass hadronic resonances. m_{T2} is defined as [78,79]

$$m_{\mathrm{T2}} = \min_{\mathbf{p}_{\mathrm{T}}^1 + \mathbf{p}_{\mathrm{T}}^2 = \mathbf{p}_{\mathrm{T}}^{\mathrm{miss}}} \{\max[m_{\mathrm{T}}(\mathbf{p}_{\mathrm{T}}^a, \mathbf{p}_{\mathrm{T}}^1), m_{\mathrm{T}}(\mathbf{p}_{\mathrm{T}}^b, \mathbf{p}_{\mathrm{T}}^2)]\}, \quad (8)$$

where $m_{\mathrm{T}}(\mathbf{p}_{\mathrm{T}}^i, \mathbf{p}_{\mathrm{T}}^j) = \sqrt{2(p_{\mathrm{T}}^i p_{\mathrm{T}}^j - \mathbf{p}_{\mathrm{T}}^i \cdot \mathbf{p}_{\mathrm{T}}^j)}$, and $\mathbf{p}_{\mathrm{T}}^a$ and $\mathbf{p}_{\mathrm{T}}^b$ are the transverse momenta of two visible particles in the decay chain, which are the two leptons in our case. $\mathbf{p}_{\mathrm{T}}^1$ and $\mathbf{p}_{\mathrm{T}}^2$ are a partition of the missing transverse momentum $\mathbf{p}_{\mathrm{T}}^{\mathrm{miss}}$. As m_{T2} is the minimum of the larger m_{T} over all partitions, its distribution for a pair production process with two semi-invisible decay chains has an upper endpoint, which is determined by the mass difference between the parent particle and its invisible child. We use three thresholds for the m_{T2} cut, aiming at varied mass splittings between $\tilde{\chi}_1^\pm$ and $\tilde{\chi}_1^0$.

Figure 4 shows the m_{SFOS} and m_{T2} distributions after the basic cuts except $|m_{\mathrm{SFOS}} - m_Z| > 10$ GeV. For the ZZ and WZ backgrounds, there can be a SFOS lepton pair induced by one Z boson. This leads to peaks around m_Z in the m_{SFOS} distributions, which are distinct in Fig. 5. The condition $|m_{\mathrm{SFOS}} - m_Z| > 10$ GeV aims at excluding such events. For BP1, these is also a peak around m_Z induced by $\tilde{\chi}_1^\pm \tilde{\chi}_2^0$ production, which, however, is not the target of the $2l + \not{E}_{\mathrm{T}}$ search. As illustrated in Fig. 5(b), the m_{T2} distributions for the WW and $t\bar{t}$ backgrounds are essentially

TABLE III. Visible cross sections σ (in fb) and signal significances (S) after each cut in the $2l + \not{E}_{\mathrm{T}}$ channel at the 14 TeV LHC. The signal significances correspond to an integrated luminosity of 300 fb^{-1}.

	WZ	ZZ	WW	$t\bar{t}$	BP1		BP2		BP3	
	σ	σ	σ	σ	σ	$\mathcal{S}$	σ	$\mathcal{S}$	σ	$\mathcal{S}$
Basic cuts	88.8	22.3	1798	8930	16.8	0.015	9.75	0.009	12.7	0.012
Jet veto	35.8	7.25	848	253	8.23	0.072	5.42	0.047	6.86	0.060
$m_{\mathrm{T2}} > 90$ GeV	0.24	0.32	0.48	0.98	0.58	2.608	0.05	0.229	0.13	0.594

bounded by m_W, while that for BP1 extends to higher values.

Table III demonstrates visible cross sections and signal significances after each cut at the 14 TeV LHC. Because b-jets are always produced associating with the two leptons in the $t\bar{t}$ background, the veto on jets kills ~97% events of this background. The $m_{\mathrm{T2}} > 90$ GeV cut is pretty powerful in suppressing the WW and $t\bar{t}$ backgrounds, reducing them by 2–3 orders of magnitude. Through these cuts, the significance of BP1 reaches above 2.6σ for 300 fb^{-1} of data. For BP2 and BP3, $m_{\tilde{\chi}_1^\pm} - m_{\tilde{\chi}_1^0} < m_W$, leading to $m_{\tilde{\chi}_1^\pm}$ decays into off-shell W bosons and hence soft m_{T2} distributions. Although the m_{T2} cut seems to discard some signal events, this condition is necessary. If not, the Drell-Yan background $pp \to l^+l^-$ would be enormous, because we have not included a $\not{E}_{\mathrm{T}}$ cut in the basic cuts. Actually, the m_{T2} cut here also serves as a $\not{E}_{\mathrm{T}}$ cut.

The expected exclusion on the parameter points at $\sqrt{s} =$ 13 and 14 TeV has been shown in Fig. 3(b). With an integrated luminosity of 30(300) fb^{-1}, the LHC $2l + \not{E}_{\mathrm{T}}$ search could reach up to $m_{\tilde{\chi}_2^0 \tilde{\chi}_1^\pm} \sim 280(480)$ GeV. However, many parameter points with $m_{\tilde{\chi}_1^\pm} - m_{\tilde{\chi}_1^0} \lesssim m_W$, as well as BP2 and BP3, are not able to be probed because their m_{T2} distributions cannot extend much beyond m_W.

IV. DIRECT AND INDIRECT DETECTION

In this section, we investigate the constraints from DM direct and indirect searches on the singlino-Higgsino scenario, as well as the sensitivity of future experiments.

A. Direct detection

DM direct detection experiments search for recoil signals of target nuclei scattered off by incident DM particles. DM-nucleus scatterings can be classified into two types, spin independent (SI) and spin dependent (SD). The SI scattering cross section is coherently enhanced by the square of the nucleon number in the nucleus. SD scatterings have no such enhancement and depend on the particular spin property of the target nucleus. Therefore, current direct detection experiments are much more sensitive to SI scatterings than SD scatterings.

Because of the Majorana nature, neutralino DM cannot have SI scatterings through the exchange of a Z boson. Nevertheless, in the singlino-Higgsino scenario SI scatterings can be induced by the Higgs boson exchange, while SD scatterings can be induced by the Z boson exchange. The SI DM-proton cross section σ_p^{SI} and the SD DM-proton cross section σ_p^{SD} for the parameter points are shown in Figs. 6(a) and 6(c), respectively. σ_p^{SD} is typically larger than σ_p^{SI} by ~2–6 orders of magnitude.

When $\Omega_{\tilde{\chi}_1^0} h^2 < 0.107$, the possibility that just a faction of DM particles are contributed by $\tilde{\chi}_1^0$ should be taken into account. For this reason, we introduce a density fraction defined by $\xi = \min(1, \Omega_{\tilde{\chi}_1^0} h^2 / 0.107)$. In this case, the proper quantities for comparing with experimental results are the reduced SI and SD cross sections, $\xi\sigma_p^{\mathrm{SI}}$ and $\xi\sigma_p^{\mathrm{SD}}$, which are shown in Figs. 6(b) and 6(d), respectively. As we can see from the left panel of Fig. 1, the predicted relic density can be very low when $\tilde{\chi}_1^0$ could annihilate through the Z or SM-like Higgs resonance. Thus, ξ can be as small as $\sim\mathcal{O}(10^{-3})$ and significantly reduce $\xi\sigma_p^{\mathrm{SI}}$ and $\xi\sigma_p^{\mathrm{SD}}$.

In Fig. 6(d), some points align as two curves reflecting the profiles of the Z and SM-like Higgs resonances. Since the singlino does not couple to Z, σ_p^{SD} is proportional to the Higgsino components of $\tilde{\chi}_1^0$. When the resonance enhancement works, $\Omega_{\tilde{\chi}_1^0} h^2$ is basically inversely proportional to the Higgsino components in the Z resonance case, as well as in the SM-like Higgs resonance case if the SM-like Higgs is doublet dominated. Consequently, $\xi\sigma_p^{\mathrm{SD}}$ can be a quantity independent of how large the Higgsino components are, and hence reflects the resonance structure. On the other hand, this behavior is not obvious in Fig. 6(b), as σ_p^{SI} is generally determined by both the singlino and Higgsino components.

In Figs. 6(a) and 6(b), we also plot the exclusion limit from LUX [80], PandaX [81], and the projected exclusion limit for XENON1T [82] in 2t · year exposure at 90% C.L. for the SI scattering. When the ξ factor is not considered, the PandaX limit excludes a lot of parameter points, especially the bunch with $m_{\tilde{\chi}_1^0} \gtrsim 100$ GeV. After considering the ξ factor, roughly half of the points in this bunch can escape from the PandaX limit, as ξ for them is typically $\sim\mathcal{O}(10^{-1})$. Nevertheless, they are covered in the XENON1T search. BP2 and BP3 have already been excluded by the PandaX search, and it is quite promising to probe BP1 in the near future experiments. When $\tilde{\chi}_1^0$ can annihilate through a resonance, no matter if it is a Z, SM-like Higgs, or other Higgs resonance, an acceptable relic density and a small DM-nucleon scattering cross section could be simultaneously obtained. In this case, there are many points that can evade the PandaX and XENON1T limits, but most of them will be well investigated in future LHC searches. For the SD scattering, the most stringent bounds come from the bubble chamber experiment PICO [83,84], as plotted in Figs. 6(c) and 6(d). Although these bounds seem quite weak, they have excluded BP3. The 90% C.L. expected exclusion limit of LZ [86] in 5.6t · 1000 day exposure will cover down to the SD cross section of $\sim 10^{-41}$ cm^2 and well investigate the singlino-Higgsino scenario.

B. Indirect detection

As an independent approach to reveal the nature of DM, indirect detection experiments seek high energy comic rays, gamma rays, and neutrinos induced by DM decays or annihilations in galactic and extragalactic objects. For

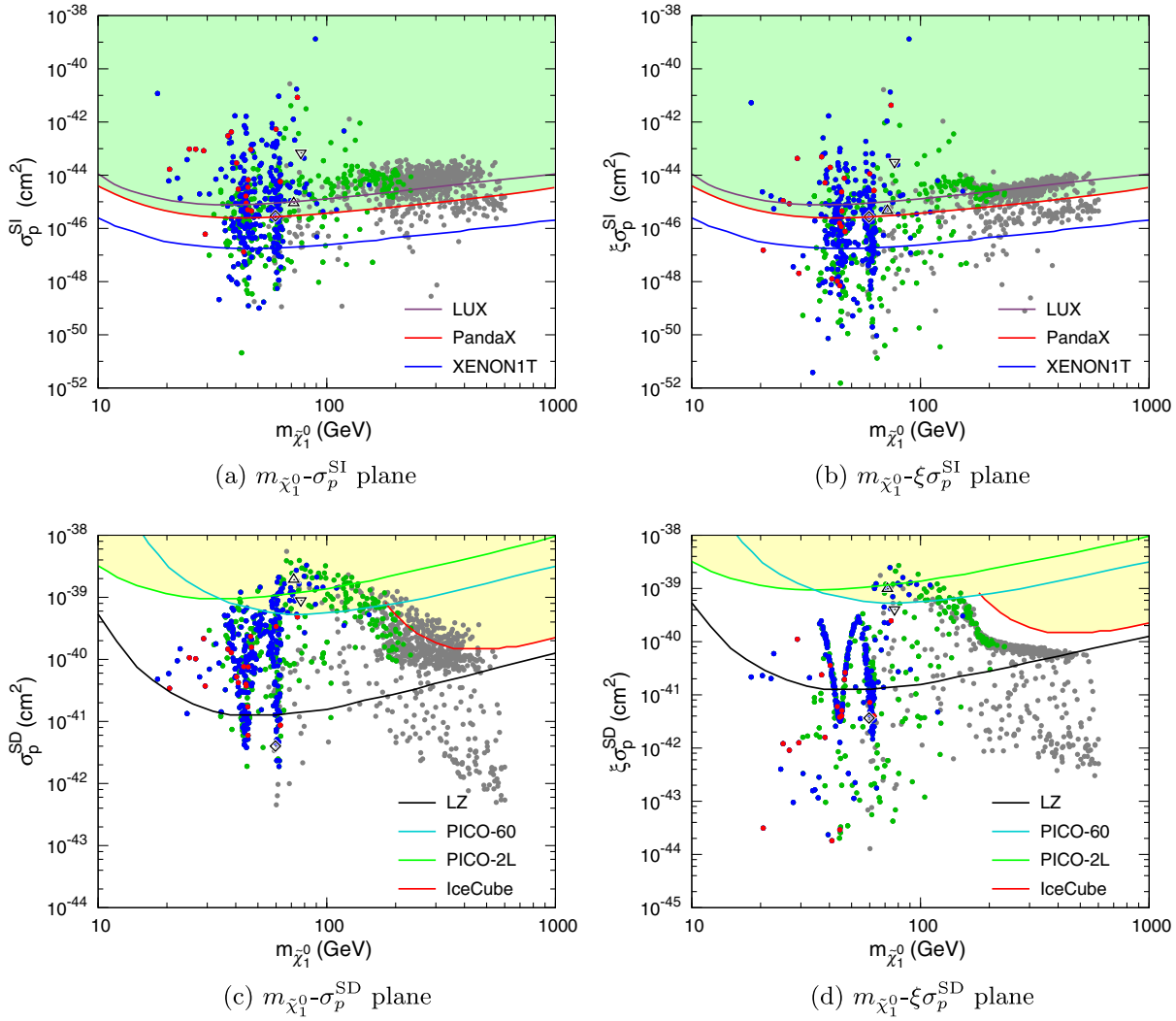

(a) $m_{\tilde{\chi}_1^0}$-σ_p^{SI} plane (b) $m_{\tilde{\chi}_1^0}$-$\xi\sigma_p^{\mathrm{SI}}$ plane

(c) $m_{\tilde{\chi}_1^0}$-σ_p^{SD} plane (d) $m_{\tilde{\chi}_1^0}$-$\xi\sigma_p^{\mathrm{SD}}$ plane

FIG. 6. Parameter points projected into the $m_{\tilde{\chi}_1^0} - \sigma_p^{\mathrm{SI}}$ (a), $m_{\tilde{\chi}_1^0} - \xi\sigma_p^{\mathrm{SI}}$ (b), $m_{\tilde{\chi}_1^0} - \sigma_p^{\mathrm{SD}}$ (c), and $m_{\tilde{\chi}_1^0} - \xi\sigma_p^{\mathrm{SD}}$ (d) planes. The notation for the colored points is the same as in Fig. 3, while open diamonds, downward triangles, and upward triangles denote BP1, BP2, and BP3, respectively. For the SI scattering, the exclusion limit from LUX [80], PandaX [81], and the expected exclusion limit of XENON1T [82] at 90% C.L. are shown. For the SD scattering, the exclusion limits from PICO [83,84] and IceCube [85] and the expected exclusion limit of LZ [86] at 90% C.L. are shown.

R-parity conserved SUSY models, the LSP is absolutely stable. Thus, indirect detection signatures come from LSP annihilation, which depends on the thermally averaged annihilation cross section $\langle\sigma_{\mathrm{ann}}v\rangle$ and the DM density in annihilation regions.

As discussed in Sec. II, for $m_{\tilde{\chi}_1^0} \lesssim 70$ GeV, a large $\langle\sigma_{\mathrm{ann}}v\rangle$ at the freeze-out epoch is mainly achieved by the resonance enhancement of a Z or Higgs boson. However, the annihilation behavior at low velocities can be quite different and the cross section can be significantly suppressed. One reason for this is that the s-wave annihilation cross section into a fermion pair $f\bar{f}$ through an s-channel Z is helicity suppressed and proportional to $m_f^2/m_{\tilde{\chi}_1^0}^2$. Additionally, the leading order of annihilation through an s-channel CP-even Higgs is of p wave. Moreover, when annihilation into $f\bar{f}$ comes through an s-channel (CP-even or CP-odd) Higgs boson, the coefficient of any wave is proportional to $m_f^2/m_{\tilde{\chi}_1^0}^2$ due to the fermion couplings to neutral Higgs bosons.

Branching fractions of major annihilation channels for nonrelativistic DM with $\sqrt{\langle v^2\rangle} = 0.001$ are shown in Fig. 7. For $m_{\tilde{\chi}_1^0} < m_t$, the dominant annihilation channel is basically either $b\bar{b}$ or a_1h_1. When both a_1 and h_1 are light, the a_1h_1 channel can be important at low velocities, although it could not compete with the $f\bar{f}$ channels at the freeze-out epoch. This channel does not suffer from helicity suppression in contrast to $f\bar{f}$. When the a_1h_1 channel is not available, the $b\bar{b}$ channel is the most important one because the b quark is the heaviest SM fermion except for the

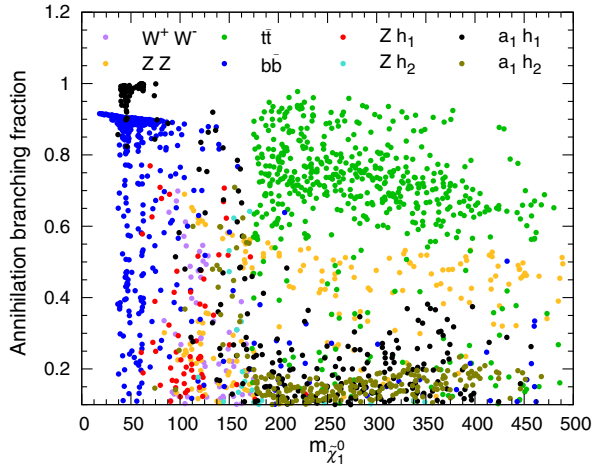

FIG. 7. Branching fractions of major $\tilde{\chi}_1^0\tilde{\chi}_1^0$ annihilation channels with $\sqrt{\langle v^2\rangle} = 0.001$.

t quark. At the freeze-out epoch, if the Z resonance enhancement was important, the annihilations into five types of light quarks were comparable to each other because p-wave annihilation was significant. However, as the DM velocity goes down, the $b\bar{b}$ channel becomes dominant over others.

For $m_{\tilde{\chi}_1^0} > m_t$, the $t\bar{t}$ channel opens and becomes dominant. It is less suppressed in the s wave, because m_t has the same order of magnitude as the $m_{\tilde{\chi}_1^0}$ value we are concerned with in this paper. Thus $\langle\sigma_{\rm ann}v\rangle$ in this channel at low velocities can be as large as that at the freeze-out epoch. Figure 8 shows that $\langle\sigma_{\rm ann}v\rangle$ for $m_{\tilde{\chi}_1^0} > m_t$ basically has a canonical value, $\sim 10^{-26}$ cm^3 s^{-1}. Nevertheless, the importance of the $t\bar{t}$ channel goes down slowly as $m_{\tilde{\chi}_1^0}$ increases, while the importance of the a_1h_1 and a_1h_2 channels slightly goes up.

The WW, ZZ, Zh_1, and Zh_2 channels typically appear as minor channels, except for some cases in a mass window of 50 GeV $\lesssim m_{\tilde{\chi}_1^0} < m_t$. This is because $m_{\tilde{\chi}_1^0}$ is singlino dominated and the singlino does not couple to electroweak gauge bosons. Actually, the $t\bar{t}$ channel is primarily contributed to by the s-channel a_1 process, rather than the s-channel Z process.

Searches for high energy muon neutrinos from DM annihilation in the center of the Sun are sensitive to the DM-proton scattering cross section, which is connected to the DM capture process in the Sun and is balanced with the annihilation rate. For the SD scattering, which is dominant for the capture of $\tilde{\chi}_1^0$, the 90% C.L. exclusion limit from the neutrino telescope IceCube [85] is more stringent than those from direct detection experiments for $m_{\tilde{\chi}_1^0} > m_t$, as plotted in Figs. 6(c) and 6(d). Note that this limit is derived under the assumption that $\tilde{\chi}_1^0\tilde{\chi}_1^0$ annihilate into $t\bar{t}$ with a branching fraction of 100%, which should be a good approximation because $t\bar{t}$ annihilation is dominant for $m_{\tilde{\chi}_1^0} > m_t$, as shown in Fig. 8. It excludes some points when the ξ factor is not taken into account.

High energy continuous gamma-ray observation is also a robust way to search for nonrelativistic DM signatures. The yield of gamma rays induced by DM depends on the annihilation rate, which is proportional to $\langle\sigma_{\rm ann}v\rangle$ and the square of DM density. Therefore, when we consider only a fraction ξ of DM is contributed to by $\tilde{\chi}_1^0$, we should use the reduced annihilation cross section $\xi^2\langle\sigma_{\rm ann}v\rangle$ to compare with experimental results. Figure 8 demonstrates the survived points projected into the $m_{\tilde{\chi}_1^0} - \langle\sigma_{\rm ann}v\rangle$ and

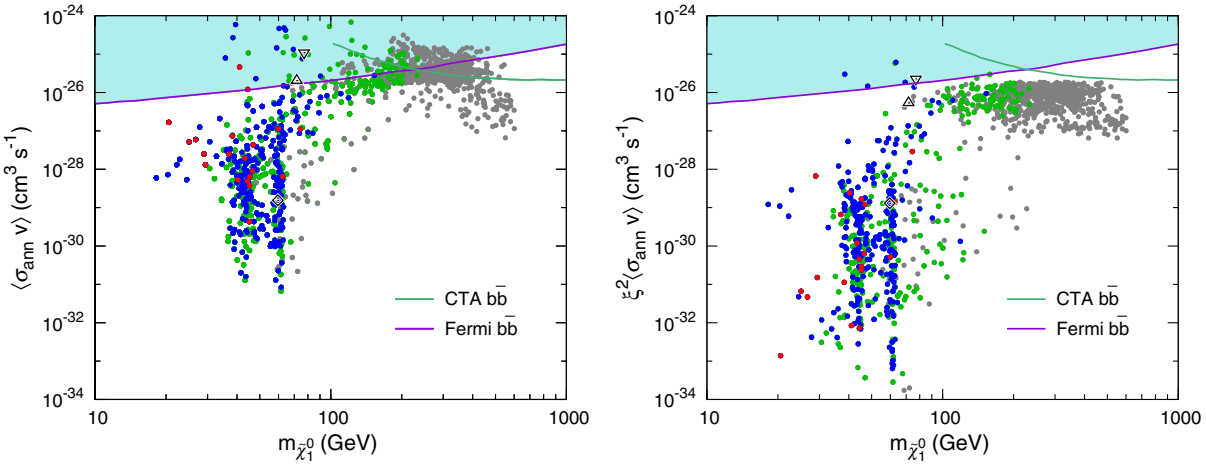

(a) $m_{\tilde{\chi}_1^0}$-$\langle\sigma_{\rm ann}v\rangle$ plane (b) $m_{\tilde{\chi}_1^0}$-$\xi^2\langle\sigma_{\rm ann}v\rangle$ plane

FIG. 8. Parameter points projected into the $m_{\tilde{\chi}_1^0} - \langle\sigma_{\rm ann}v\rangle$ (a) and $m_{\tilde{\chi}_1^0} - \xi^2\langle\sigma_{\rm ann}v\rangle$ (b) planes. The notation for the points is the same as in Fig. 6. For a comparison, we also plot the exclusion limit from the Fermi-LAT gamma-ray observation of dwarf galaxies [87] and the expected exclusion limit for the CTA 100-hour observation of the Galactic center vicinities [88] at 95% C.L., assuming that $\tilde{\chi}_1^0$ pairs only annihilate into $b\bar{b}$.

$m_{\tilde{\chi}_1^0} - \xi^2\langle\sigma_{\rm ann}v\rangle$ planes with $\sqrt{\langle v^2\rangle} = 0.001$. All annihilation channels are included. For $m_{\tilde{\chi}_1^0} \lesssim 70$ GeV, because the resonant channels that efficiently worked at the freeze-out epoch are suppressed by the velocity, $\langle\sigma_{\rm ann}v\rangle$ with $\sqrt{\langle v^2\rangle} = 0.001$ has a value of $\sim\mathcal{O}(10^{-31})$–$\mathcal{O}(10^{-27})$ cm^3 s^{-1}, much smaller than the canonical value.

In Fig. 8 we also plot the exclusion limit from the Fermi-LAT gamma-ray observation of dwarf galaxies [87] and the expected exclusion limit for the CTA 100-hour observation of the Galactic center vicinities [88] at 95% C.L. Both limits are based on the assumption that $\tilde{\chi}_1^0\tilde{\chi}_1^0$ annihilate into $b\bar{b}$ with a branching fraction of 100%. In principle, the gamma-ray spectra induced by different annihilation channels are different. Here the dominant channels include $b\bar{b}$, $t\bar{t}$, $a_1h_{1,2}$, W^+W^-, and $Zh_{1,2}$. The gamma-ray spectra from these channels are quite similar [89], since they all go through the hadronization process, which is universal, and yield most photons from hadron decays. Therefore, although the limits are set for the $b\bar{b}$ channel, they should be good approximations for the real situation. Figure 8 shows that the Fermi-LAT limit can exclude some points but not so many, while the CTA experiment will be complementary to Fermi-LAT, as it will be more sensitive in the high mass region. When the ξ^2 factor is considered, as shown in Fig. 8(b), almost all the points evade these limits. This means that indirect searches for continuous gamma rays may not be an effective way to explore the singlino-Higgsino scenario, compared with direct detection and collider searches.

V. CONCLUSIONS AND DISCUSSIONS

In this work, we explore the singlino-Higgsino scenario in the NMSSM, where the singlino and Higgsinos are light and decouple from other superpartners. We assume that the LSP neutralino $\tilde{\chi}_1^0$ is singlino dominated, while $\tilde{\chi}_2^0$ and $\tilde{\chi}_3^0$ are mainly Higgsinos. Furthermore, the lighter chargino $\tilde{\chi}_1^\pm$ is a complete Higgsino, with a mass close to $\tilde{\chi}_2^0$ and $\tilde{\chi}_3^0$. This setup is distinct from any simplified scenario in the MSSM, as the singlet superfield plays an important role in dark matter phenomenology and collider physics. In order to satisfy the observed DM relic abundance, the LSP should have either resonant annihilation effects or sizable Higgsino components, due to the limited interactions of the singlino.

We carry out a random scan in the parameter space to obtain realistic parameters. Three benchmark points are picked up to represent typical cases with different neutralino decay modes. As represented by BP1, in most cases $\tilde{\chi}_{2,3}^0$ dominantly decays into $\tilde{\chi}_1^0 Z$ and $\tilde{\chi}_1^\pm$ decays into $\tilde{\chi}_1^0 W^\pm$. Therefore, the $3l + \not{E}_{\rm T}$ and $2l + \not{E}_{\rm T}$ searches at the LHC are expected to be sensitive to $\tilde{\chi}_1^\pm\tilde{\chi}_{2,3}^0$ and $\tilde{\chi}_1^+\tilde{\chi}_1^-$ direct production with clean SM backgrounds. We recast the 8 TeV LHC search results and find that the exclusion limit reaches up to $m_{\tilde{\chi}_2^0,\tilde{\chi}_1^\pm} \sim 250$ GeV. Based on a detailed simulation, the prospect of future LHC searches is also investigated. With an integrated luminosity of 30(300) fb^{-1} at $\sqrt{s} =$ 13(14) TeV, LHC searches are expected to probe up to $m_{\tilde{\chi}_2^0,\tilde{\chi}_1^\pm} \sim 320(480)$ GeV and $m_{\tilde{\chi}_1^0} \sim 150(230)$ GeV.

The $3l + \not{E}_{\rm T}$ and $2l + \not{E}_{\rm T}$ searches lose their sensitivities for the compressed mass spectra where $m_{\tilde{\chi}_{2,3}^0,\tilde{\chi}_1^\pm} - m_{\tilde{\chi}_1^0} \lesssim m_{Z,W}$. This case is typically represented by BP2 and BP3, where $\tilde{\chi}_{2,3}^0$ dominantly decays into $\tilde{\chi}_1^0 h_1$ or $\tilde{\chi}_1^0 a_1$, while $\tilde{\chi}_1^\pm$ decays into off-shell W bosons. Consequently, distinct $3l + \not{E}_{\rm T}$ and $2l + \not{E}_{\rm T}$ final states would not be easily established. Since the dominant decay channel of h_1 and a_1 here is $b\bar{b}$, the $2b$-jets $+ 1l + \not{E}_{\rm T}$ final state provides a particular signature of $\tilde{\chi}_1^\pm\tilde{\chi}_{2,3}^0$ production. However, this search channel would be very challenging due to the enormous $t\bar{t}$ background.

Furthermore, we study current bounds and future sensitivities of DM direct and indirect detection experiments. Unlike collider searches, direct and indirect detection can keep sensitive to heavy LSPs with $m_{\tilde{\chi}_1^0} > 250$ GeV. Compressed mass spectra are no longer an issue, for instance; BP2 and BP3 have been excluded by current direct detection experiments. When the LSPs annihilated through a Z or Higgs resonance in the early Universe to achieve an acceptable relic abundance, its Higgsino components could be very tiny, leading to small DM-nuclei scattering cross sections as well as small nonrelativistic annihilation cross sections. Thus, this is a difficult case for direct and indirect searches. Fortunately, most parameter points in this case would be covered by the LHC $3l + \not{E}_{\rm T}$ and $2l + \not{E}_{\rm T}$ searches, as long as $m_{\tilde{\chi}_2^0,\tilde{\chi}_1^\pm} \lesssim 480$ GeV. Therefore, we conclude that the singlino-Higgsino scenario will be very well investigated in near future LHC searches and DM detection experiments.

ACKNOWLEDGMENTS

This work is supported by the National Natural Science Foundation of China under Grants No. 11475189, No. 11475191, and No. 11135009, the 973 Program of China under Grant No. 2013CB837000, and by the Strategic Priority Research Program "The Emergence of Cosmological Structures" of the Chinese Academy of Sciences under Grant No. XDB09000000. Z. H. Y. is supported by the Australian Research Council.

[1] G. Aad *et al.* (ATLAS Collaboration), Observation of a new particle in the search for the standard model Higgs boson with the ATLAS detector at the LHC, Phys. Lett. B **716**, 1 (2012).

[2] S. Chatrchyan *et al.* (CMS Collaboration), Observation of a new boson at a mass of 125 GeV with the CMS experiment at the LHC, Phys. Lett. B **716**, 30 (2012).

[3] J. E. Kim and H. P. Nilles, The mu problem and the strong CP problem, Phys. Lett. **138B**, 150 (1984).

[4] M. Bastero-Gil, C. Hugonie, S. F. King, D. P. Roy, and S. Vempati, Does LEP prefer the NMSSM?, Phys. Lett. B **489**, 359 (2000).

[5] R. Kitano and Y. Nomura, Supersymmetry, naturalness, and signatures at the LHC, Phys. Rev. D **73**, 095004 (2006).

[6] M. Papucci, J. T. Ruderman, and A. Weiler, Natural SUSY endures, J. High Energy Phys. 09 (2012) 035.

[7] J.-J. Cao, Z.-X. Heng, J. M. Yang, Y.-M. Zhang, and J.-Y. Zhu, A SM-like Higgs near 125 GeV in low energy SUSY: a comparative study for MSSM and NMSSM, J. High Energy Phys. 03 (2012) 086.

[8] Z. Kang, J. Li, and T. Li, On naturalness of the MSSM and NMSSM, J. High Energy Phys. 11 (2012) 024.

[9] M. Maniatis, The next-to-minimal supersymmetric extension of the standard model reviewed, Int. J. Mod. Phys. A **25**, 3505 (2010).

[10] U. Ellwanger, C. Hugonie, and A. M. Teixeira, The next-to-minimal supersymmetric standard model, Phys. Rep. **496**, 1 (2010).

[11] G. Aad *et al.* (ATLAS Collaboration), Summary of the searches for squarks and gluinos using $\sqrt{s} = 8$ TeV pp collisions with the ATLAS experiment at the LHC, J. High Energy Phys. 10 (2015) 054.

[12] G. Aad *et al.* (ATLAS Collaboration), Summary of the ATLAS experiment sensitivity to supersymmetry after LHC run 1 interpreted in the phenomenological MSSM, J. High Energy Phys. 10 (2015) 134.

[13] V. Khachatryan *et al.* (CMS Collaboration), Searches for supersymmetry using the M_{T2} variable in hadronic events produced in pp collisions at 8 TeV, J. High Energy Phys. 05 (2015) 078.

[14] G. Aad *et al.* (ATLAS Collaboration), Search for direct production of charginos and neutralinos in events with three leptons and missing transverse momentum in $\sqrt{s} = 8$ TeV pp collisions with the ATLAS detector, J. High Energy Phys. 04 (2014) 169.

[15] G. Aad *et al.* (ATLAS Collaboration), Search for direct production of charginos, neutralinos and sleptons in final states with two leptons and missing transverse momentum in pp collisions at $\sqrt{s} = 8$ TeV with the ATLAS detector, J. High Energy Phys. 05 (2014) 071.

[16] G. Aad *et al.* (ATLAS Collaboration), Search for the electroweak production of supersymmetric particles in $\sqrt{s} = 8$ TeV pp collisions with the ATLAS detector, Phys. Rev. D **93**, 052002 (2016).

[17] G. Aad *et al.* (ATLAS Collaboration), Search for direct pair production of a chargino and a neutralino decaying to the 125 GeV Higgs boson in $\sqrt{s} = 8$ TeV pp collisions with the ATLAS detector, Eur. Phys. J. C **75**, 208 (2015).

[18] V. Khachatryan *et al.* (CMS Collaboration), Searches for electroweak production of charginos, neutralinos, and sleptons decaying to leptons and W, Z, and Higgs bosons in pp collisions at 8 TeV, Eur. Phys. J. C **74**, 3036 (2014).

[19] V. Khachatryan *et al.* (CMS Collaboration), Searches for electroweak neutralino and chargino production in channels with Higgs, Z, and W bosons in pp collisions at 8 TeV, Phys. Rev. D **90**, 092007 (2014).

[20] A. Fowlie, K. Kowalska, L. Roszkowski, E. M. Sessolo, and Y.-L. S. Tsai, Dark matter and collider signatures of the MSSM, Phys. Rev. D **88**, 055012 (2013).

[21] S. Gori, S. Jung, and L.-T. Wang, Cornering electroweakinos at the LHC, J. High Energy Phys. 10 (2013) 191.

[22] T. Han, S. Padhi, and S. Su, Electroweakinos in the light of the Higgs boson, Phys. Rev. D **88**, 115010 (2013).

[23] P. Schwaller and J. Zurita, Compressed electroweakino spectra at the LHC, J. High Energy Phys. 03 (2014) 060.

[24] S. P. Das, M. Guchait, and D. P. Roy, Testing SUSY models for the muon g-2 anomaly via chargino-neutralino pair production at the LHC, Phys. Rev. D **90**, 055011 (2014).

[25] T. A. W. Martin and D. Morrissey, Electroweakino constraints from LHC data, J. High Energy Phys. 12 (2014) 168.

[26] L. Calibbi, J. M. Lindert, T. Ota, and Y. Takanishi, LHC tests of light neutralino dark matter without light sfermions, J. High Energy Phys. 11 (2014) 106.

[27] C. Han, L. Wu, J. M. Yang, M. Zhang, and Y. Zhang, New approach for detecting a compressed bino/wino at the LHC, Phys. Rev. D **91**, 055030 (2015).

[28] C. Han, Probing light bino and Higgsinos at the LHC, arXiv:1409.7000.

[29] G. Grilli di Cortona, Hunting electroweakinos at future hadron colliders and direct detection experiments, J. High Energy Phys. 05 (2015) 035.

[30] M. Chakraborti, U. Chattopadhyay, A. Choudhury, A. Datta, and S. Poddar, Reduced LHC constraints for Higgsinolike heavier electroweakinos, J. High Energy Phys. 11 (2015) 050.

[31] A. Nelson, P. Tanedo, and D. Whiteson, Limiting SUSY compressed spectra scenarios, Phys. Rev. D **93**, 115029 (2016).

[32] J. Bramante, N. Desai, P. Fox, A. Martin, B. Ostdiek, and T. Plehn, Towards the final word on neutralino dark matter, Phys. Rev. D **93**, 063525 (2016).

[33] M. Badziak, A. Delgado, M. Olechowski, S. Pokorski, and K. Sakurai, Detecting underabundant neutralinos, J. High Energy Phys. 11 (2015) 053.

[34] A. Chakraborty, D. K. Ghosh, S. Mondal, S. Poddar, and D. Sengupta, Probing the NMSSM via Higgs boson signatures from stop cascade decays at the LHC, Phys. Rev. D **91**, 115018 (2015).

[35] J. Cao, Y. He, L. Shang, W. Su, and Y. Zhang, Testing the light dark matter scenario of the MSSM at the LHC, J. High Energy Phys. 03 (2016) 207.

[36] A. Choudhury and S. Mondal, Revisiting the Exclusion Limits from Direct Chargino-Neutralino Production at the LHC, arXiv:1603.05502.

[37] M. van Beekveld, W. Beenakker, S. Caron, and R. R. de Austri, The case for 100 GeV bino dark matter: a dedicated LHC trilepton search, J. High Energy Phys. 04 (2016) 154.

[38] J. F. Gunion, D. Hooper, and B. McElrath, Light neutralino dark matter in the NMSSM, Phys. Rev. D **73**, 015011 (2006).
[39] G. Belanger, F. Boudjema, C. Hugonie, A. Pukhov, and A. Semenov, Relic density of dark matter in the NMSSM, J. Cosmol. Astropart. Phys. 09 (2005) 001.
[40] C. Hugonie, G. Belanger, and A. Pukhov, Dark matter in the constrained NMSSM, J. Cosmol. Astropart. Phys. 11 (2007) 009.
[41] J. Cao, K.-i. Hikasa, W. Wang, and J. M. Yang, Light dark matter in NMSSM and implication on Higgs phenomenology, Phys. Lett. B **703**, 292 (2011).
[42] T. Cheng and T. Li, Electroweak supersymmetry (EWSUSY) in the NMSSM, Phys. Rev. D **88**, 015031 (2013).
[43] T. Cheng, J. Li, T. Li, and Q.-S. Yan, Natural NMSSM confronting with the LHC7-8, Phys. Rev. D **89**, 015015 (2014).
[44] J. Kozaczuk and S. Profumo, Light NMSSM neutralino dark matter in the wake of CDMS II and a 126 GeV Higgs boson, Phys. Rev. D **89**, 095012 (2014).
[45] M. Badziak, M. Olechowski, and P. Szczerbiak, Blind spots for neutralino dark matter in the NMSSM, J. High Energy Phys. 03 (2016) 179.
[46] U. Ellwanger, Testing the Higgsino-singlino sector of the NMSSM with trileptons at the LHC, J. High Energy Phys. 11 (2013) 108.
[47] J. S. Kim and T. S. Ray, The Higgsino-singlino world at the large hadron collider, Eur. Phys. J. C **75**, 40 (2015).
[48] B. Dutta, Y. Gao, and B. Shakya, Light Higgsino decays as a probe of the NMSSM, Phys. Rev. D **91**, 035016 (2015).
[49] J. Cao, L. Shang, P. Wu, J. M. Yang, and Y. Zhang, Supersymmetry explanation of the Fermi Galactic center excess and its test at LHC run II, Phys. Rev. D **91**, 055005 (2015).
[50] R. Enberg, S. Munir, C. Prez de los Heros, and D. Werder, Prospects for Higgsino-singlino dark matter detection at IceCube and PINGU, arXiv:1506.05714.
[51] C. T. Potter, Natural NMSSM with a light singlet Higgs and singlino LSP, Eur. Phys. J. C **76**, 44 (2016).
[52] N. Arkani-Hamed, A. Delgado, and G. F. Giudice, The well-tempered neutralino, Nucl. Phys. **B741**, 108 (2006).
[53] J. Cao, C. Han, L. Wu, P. Wu, and J. M. Yang, A light SUSY dark matter after CDMS-II, LUX and LHC Higgs data, J. High Energy Phys. 05 (2014) 056.
[54] T. Nihei, L. Roszkowski, and R. Ruiz de Austri, Exact cross-sections for the neutralino WIMP pair annihilation, J. High Energy Phys. 03 (2002) 031.
[55] C. Beskidt, W. de Boer, D. I. Kazakov, and S. Wayand, Higgs branching ratios in constrained minimal and next-to-minimal supersymmetry scenarios surveyed, Phys. Lett. B **759**, 141 (2016).
[56] U. Ellwanger, J. F. Gunion, and C. Hugonie, NMHDECAY: a Fortran code for the Higgs masses, couplings and decay widths in the NMSSM, J. High Energy Phys. 02 (2005) 066.
[57] U. Ellwanger and C. Hugonie, NMHDECAY 2.0: an updated program for sparticle masses, Higgs masses, couplings and decay widths in the NMSSM, Comput. Phys. Commun. **175**, 290 (2006).
[58] U. Ellwanger and C. Hugonie, NMSPEC: a Fortran code for the sparticle and Higgs masses in the NMSSM with GUT scale boundary conditions, Comput. Phys. Commun. **177**, 399 (2007).
[59] G. Belanger, F. Boudjema, A. Pukhov, and A. Semenov, micrOMEGAs_3: a program for calculating dark matter observables, Comput. Phys. Commun. **185**, 960 (2014).
[60] P. Ade *et al.* (Planck Collaboration), Planck 2015 results. XIII. Cosmological parameters, arXiv:1502.01589 [Astron. Astrophys. (to be published)].
[61] J. Bernon, B. Dumont, and S. Kraml, Status of Higgs couplings after run 1 of the LHC, Phys. Rev. D **90**, 071301 (2014).
[62] S. Schael *et al.* (SLD Electroweak Group, DELPHI, ALEPH, SLD, SLD Heavy Flavour Group, OPAL, LEP Electroweak Working Group, L3 Collaboration), Precision electroweak measurements on the Z resonance, Phys. Rep. **427**, 257 (2006).
[63] G. W. Bennett *et al.* (Muon g-2 Collaboration), Measurement of the Negative Muon Anomalous Magnetic Moment to 0.7 ppm, Phys. Rev. Lett. **92**, 161802 (2004).
[64] Y. Amhis *et al.* (Heavy Flavor Averaging Group (HFAG) Collaboration), Averages of b-hadron, c-hadron, and τ-lepton properties as of summer 2014, arXiv:1412.7515.
[65] J. P. Lees *et al.* (*BABAR* Collaboration), Evidence of $B^+ \to \tau^+\nu$ decays with hadronic B tags, Phys. Rev. D **88**, 031102 (2013).
[66] W. B. Lin, D. H. Huang, X. Zhang, and R. H. Brandenberger, Nonthermal Production of WIMPs and the Subgalactic Structure of the Universe, Phys. Rev. Lett. **86**, 954 (2001).
[67] M. Fujii and K. Hamaguchi, Nonthermal dark matter via Affleck-Dine baryogenesis and its detection possibility, Phys. Rev. D **66**, 083501 (2002).
[68] G. L. Kane, P. Kumar, B. D. Nelson, and B. Zheng, Dark matter production mechanisms with a nonthermal cosmological history: a classification, Phys. Rev. D **93**, 063527 (2016).
[69] P. Salati, Quintessence and the relic density of neutralinos, Phys. Lett. B **571**, 121 (2003).
[70] F. Rosati, Quintessential enhancement of dark matter abundance, Phys. Lett. B **570**, 5 (2003).
[71] S. Profumo and P. Ullio, SUSY dark matter and quintessence, J. Cosmol. Astropart. Phys. 11 (2003) 006.
[72] K. M. Zurek, Multicomponent dark matter, Phys. Rev. D **79**, 115002 (2009).
[73] J. Alwall, R. Frederix, S. Frixione, V. Hirschi, F. Maltoni, O. Mattelaer, H. S. Shao, T. Stelzer, P. Torrielli, and M. Zaro, The automated computation of tree-level and next-to-leading order differential cross sections, and their matching to parton shower simulations, J. High Energy Phys. 07 (2014) 079.
[74] T. Sjostrand, S. Mrenna, and P. Z. Skands, PYTHIA 6.4 physics and manual, J. High Energy Phys. 05 (2006) 026.
[75] M. L. Mangano, M. Moretti, F. Piccinini, and M. Treccani, Matching matrix elements and shower evolution for top-quark production in hadronic collisions, J. High Energy Phys. 01 (2007) 013.
[76] J. de Favereau, C. Delaere, P. Demin, A. Giammanco, V. Lematre, A. Mertens, and M. Selvaggi (DELPHES 3

Collaboration), DELPHES 3, a modular framework for fast simulation of a generic collider experiment, J. High Energy Phys. 02 (2014) 057.
[77] M. Cacciari, G. P. Salam, and G. Soyez, The anti-k(t) jet clustering algorithm, J. High Energy Phys. 04 (2008) 063.
[78] C. G. Lester and D. J. Summers, Measuring masses of semi-invisibly decaying particles pair produced at hadron colliders, Phys. Lett. B **463**, 99 (1999).
[79] A. Barr, C. Lester, and P. Stephens, m(T2): the truth behind the glamour, J. Phys. G **29**, 2343 (2003).
[80] D. S. Akerib *et al.* (LUX Collaboration), First Results from the LUX Dark Matter Experiment at the Sanford Underground Research Facility, Phys. Rev. Lett. **112**, 091303 (2014).
[81] A. Tan *et al.* (PandaX-II Collaboration), Dark Matter Results from First 98.7-day Data of PandaX-II Experiment, arXiv:1607.07400.
[82] E. Aprile *et al.* (XENON Collaboration), Physics reach of the XENON1T dark matter experiment, J. Cosmol. Astropart. Phys. 04 (2016) 027.
[83] C. Amole *et al.* (PICO Collaboration), Dark Matter Search Results from the PICO-2L C_3F_8 Bubble Chamber, Phys. Rev. Lett. **114**, 231302 (2015).
[84] C. Amole *et al.* (PICO Collaboration), Dark matter search results from the PICO-60 CF_3I bubble chamber, arXiv:1510.07754 [Phys. Rev. D (to be published)].
[85] M. G. Aartsen *et al.* (IceCube Collaboration), Improved limits on dark matter annihilation in the Sun with the 79-string IceCube detector and implications for supersymmetry, arXiv:1601.00653.
[86] D. S. Akerib *et al.* (LZ Collaboration), LUX-ZEPLIN (LZ) conceptual design report, arXiv:1509.02910 [Department of Energy (to be published)].
[87] M. Ackermann *et al.* (Fermi-LAT Collaboration), Searching for dark matter annihilation from Milky Way dwarf spheroidal galaxies with six years of Fermi-LAT data, Astrophys. J. **809**, L4 (2015).
[88] M. Doro *et al.* (CTA Consortium Collaboration), Dark matter and fundamental physics with the Cherenkov Telescope Array, Astropart. Phys. **43**, 189 (2013).
[89] M. Cirelli, G. Corcella, A. Hektor, G. Hutsi, M. Kadastik, P. Panci, M. Raidal, F. Sala, and A. Strumia, PPPC 4 DM ID: a poor particle physicist cookbook for dark matter indirect detection, J. Cosmol. Astropart. Phys. 03 (2011) 051; 10 (2012) E01.